Control over hysteresis curves and thresholds of optical bistability in different semiconductor double quantum wells*

Hamedi H R[a)†], Mehmannavaz M R[b)], and Afshari Hadi[c)]

[a)] *Institute of Theoretical Physics and Astronomy, Vilnius University, A. Gostauto* 12, *LT*-01108, *Vilnius Lithuania*
[b)] *Young Researchers and Elite Club, Mashhad Branch, Islamic Azad University, Mashhad, Iran*
[c)] *Research Institute for Applied Physics, University of Tabriz, Tabriz, Iran*

(Received 6 February 2015; revised manuscript received 27 March 2015; published online 20 June 2015)

The effects of optical field on the phenomenon of optical bistability (OB) are investigated in a K-type semiconductor double quantum well (SDQW) under various parametric conditions. It is shown that the OB threshold can be manipulated by increasing the intensity of coupling field. The dependence of the shift of OB hysteresis curve on probe wavelength detuning is then explored. In order to demonstrate controllability of the OB in this SDQW, we compare the OB features of three different configurations which could arise in this SDQW scheme, i.e., K-type, Y-type, and inverted Y-type systems. The controllability of this semiconductor nanostructure medium makes the presented OB scheme more valuable for applications in all-optical switches, information storage, and logic circuits of all optical information processing.

Keywords: optical bistability, semiconductor double quantum wells, K-type, Y-type, and inverted Y-type schemes, OB threshold intensity

PACS: 42.65.Pc, 42.65.Sf, 42.68.Ay **DOI:** 10.1088/1674-1056/24/8/084211

1. Introduction

An optical system which presents two steady transmission states for the same input intensity is optically bistable. Optical bistability (OB) has been extensively studied both experimentally and theoretically in two-level atomic systems due to its wide applications such as optical transistors, memory elements, and all optical switches.[1,2] However, there are some limitations for applications because of lack of control due to only one laser beam being employed. It was realized that the influence of electromagnetically induced transparency (EIT)[3,4] not only modifies the linear optical properties of the medium,[5–10] but also can lead to nonlinear optical process[11–16] in multi-level atomic media. It is theoretically and experimentally studied that placing a multi-level EIT medium in an optical cavity to combine the nonlinear response of the sample and optical feedback of the intracavity optical field can enhance remarkably the Kerr nonlinear coefficient of the medium.[17–19] Another interesting phenomenon, controllable OB threshold and width of hysteresis curves in multi-level atomic media have been explored.[20–27]

On the other hands, in recent years, semiconductor quantum wells have drawn significant attention because they can be viewed as a two-dimensional (2D) electron gas, having properties similar to those of atomic vapors such as the discrete levels, but with the advantages of high nonlinear optical coefficients and large electric dipole moments, due to the small effective electron mass. Several typical interesting phenomena such as EIT,[28–30] highly efficient four-wave mixing,[31] all-optical switching,[32] large Kerr nonlinearity,[33–35] optical bistability,[36–40] electron localization,[41–43] etc.[44–46] have been demonstrated in these solid media. Li showed that optical bistability behavior based on intersubband transitions in asymmetric double quantum wells (QWs) where tunneling-induced quantum inference can be observed.[36] A hybrid absorptive–dispersive optical multistability (OM) behavior in a three-level ladder-type quantum well system inside a unidirectional ring cavity is investigated by Wang.[38] In this paper, the OB behavior of the K-shaped SDQW system is investigated and then, the bistable properties of this configuration are compared with those of Y- and inverted-Y-configurations. These systems in Y-type, inverted-Y, and K-type configurations are composed of two or more than two different EIT sub-systems so that it sounds interesting to compare the OB characteristics of these schemes.

2. Theoretical framework

The system under consideration is an SDQW structure consisting of two quantum wells. This structure is grown by molecular beam epitaxy on a semi-insulating GaAs substrate and comprised of fifty modulation-doped coupled-quantum wells. One period for one of the structures displayed in Fig. 1(a), which consists of two quantum wells. QW1 is deep well and has 7.0 nm in thickness, and QW2 is shallow well and has 6.0 nm in thickness, the wells separated by a 2.0-nm-thick $Al_{0.33}Ga_{0.67}As$ tunnel barrier can be grown on GaAs substrate. This barrier will couple the excited state of the deep well with the excited state of the shallow well to create a dou-

*Project supported by the Lithuanian Research Council (Grant No. VP1-3.1-ŠM-01-V-03-001).
†Corresponding author. E-mail: Hamid.r.Hamedi@gmail.com
© 2015 Chinese Physical Society and IOP Publishing Ltd

blet of states. The coupled well periods can have a separation of 95 nm by inserting another spacer layer of $Al_{0.33}Ga_{0.67}As$.

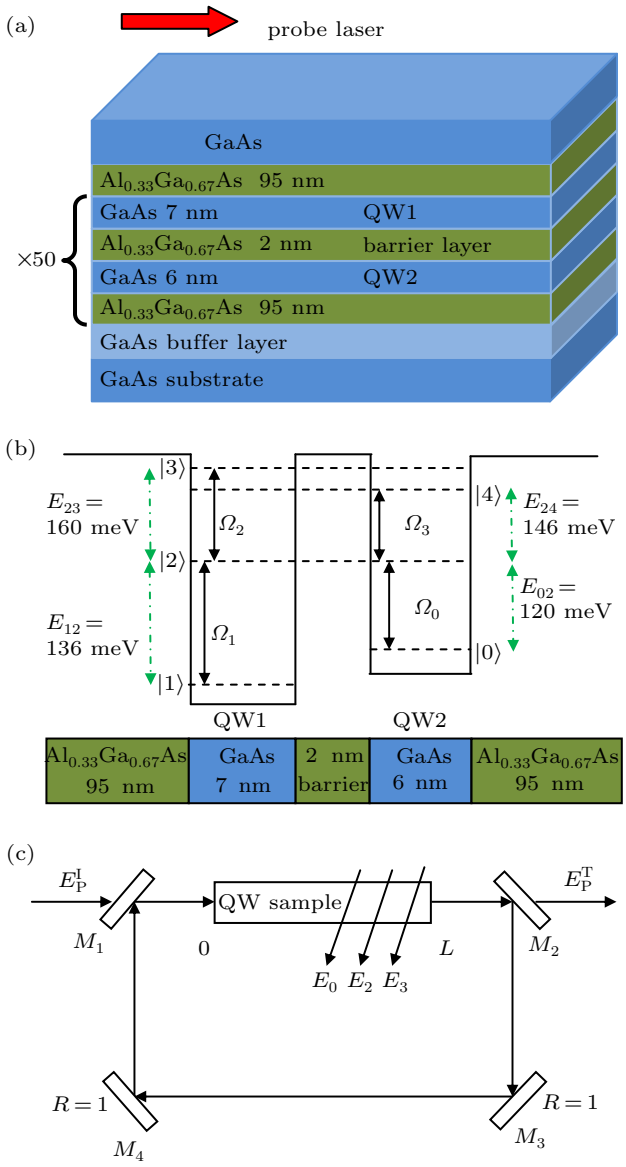


Fig. 1. (color online) (a) Cross section of GaAs/AlGaAsSDQW structure. (b) Schematic band diagram of a single period of the GaAs modulation-doped quantum well structure separated by an $Al_{0.33}Ga_{0.67}As$ barrier. (c) Schematic setup of unidirectional ring cavity containing a SDQW sample of length L, $E_p^{\rm I}$ and $E_p^{\rm T}$ are the incident and the transmitted probe fields, respectively.

This SDQW structure could be designed to meet the transition energy requirements of E_{12}= 136 meV, E_{02} = 120 meV, E_{23}= 160 meV, and E_{24} = 146 meV, which is easily accessible with an available semiconductor diode laser system in the mid-infrared range.[47–50] Since the $Al_{0.33}Ga_{0.67}As$ region is longer than the electron coherence length (λ_c: 20 nm–50 nm), it supports an energy continuum.[51] The electronic level diagram of this SDQW structure system is shown in Fig. 1(b).

2.1. K-type system

This system consists of five subbands that constitute a K-type system as shown in Fig. 2(a), and is similar to the integration of the two systems V-type and Λ-type that are connected by a common-level $|2\rangle$. Here, levels $|1\rangle$, $|2\rangle$, and $|0\rangle$ are in a usual three-level Λ-type configuration and level $|2\rangle$ together with levels $|3\rangle$ and $|4\rangle$ forms a three-level V-type configuration. The description of the optically allowed transitions in this system is as follows. The transition $|1\rangle$ to $|2\rangle$ with transition frequency ω_{12} interacts with a weak probe field (with amplitude E_1 and frequency ω_1) having Rabi-frequency $\Omega_1 = E_1.\mu_{12}/2\hbar$ (where μ_{ij} is the dipole moment between the states $|i\rangle$ and $|j\rangle$). A coupling field with amplitude E_0 (frequency ω_0) drives the transition $|0\rangle$ to $|2\rangle$ (transition frequency ω_{02}) with the Rabi-frequency $\Omega_0 = E_0.\mu_{02}/2\hbar$, while a pumping field with amplitude E_2 (frequency ω_2) and Rabi-frequency $\Omega_2 = E_2.\mu_{23}/2\hbar$ acts on the transition $|2\rangle$ to $|3\rangle$ (with transition frequency ω_{32}). The second pumping field with amplitude E_3 (frequency ω_3) acts on the transition $|2\rangle$ to $|4\rangle$ (with transition frequency ω_{24}) having the Rabi- frequency equal to $\Omega_3 = E_3.\mu_{24}/2\hbar$.

The total decay rates for subbands are γ_i, $(i = 0, 1, 2, 3, 4)$. In semiconductor quantum wells, the overall decay rate γ_i of subband $|i\rangle$ comprises a population-decay contribution as well as a dephasing contribution. The first term, i.e., the population-decay contribution is due primarily to longitudinal optical (LO) photon emission events at low temperature, while the second term (dephasing contribution) depends on electron–electron scattering, electron–phonon scattering, and inhomogeneous broadening due to scattering on interface roughness, which is added phenomenologically into the above density-matrix equations.[52–54] The corresponding detunings for these transitions are $\Delta_1 = \omega_1 - \omega_{12}$, $\Delta_0 = \omega_0 - \omega_{02}$, $\Delta_2 = \omega_2 - \omega_{23}$, and $\Delta_3 = \omega_3 - \omega_{24}$, respectively. The probe laser field detuning with respect to the QW transition frequency $|1\rangle \leftrightarrow |2\rangle$ is $\Delta_1 = \omega_1 - \omega_{12}$, and using the corresponding wavelengths the frequencies are expressed as $\omega_1 = 2\pi c/\lambda$ and $\omega_{12} = 2\pi c/\lambda_0$. We take $\lambda = 1550$ μm in our study that is the most important wavelength in communication applications.

Using the method developed in Refs. [55] and [56] in the rotating-wave approximation (RWA), the total Hamiltonian describing the interaction of the probe and control fields with the SDQW structure system can be expressed as

$$H = H_0 + H_1, \tag{1}$$

where H_0 is the free energy part, and H_1 is the interaction Hamiltonian of the SDQW system with the probe and controls fields. The detailed form of these terms can be written as

$$\begin{aligned} H_0 &= \hbar\nu_0 |0\rangle\langle 0| + \hbar\nu_1 |1\rangle\langle 1| + \hbar\nu_2 |2\rangle\langle 2| \\ &\quad + \hbar\nu_3 |3\rangle\langle 3| + \hbar\nu_4 |4\rangle\langle 4|, \end{aligned} \tag{2}$$

$$\begin{aligned} H_1 &= -\hbar\Omega_1 e^{-i\omega_1 t} |2\rangle\langle 1| - \hbar\Omega_0 e^{-i\omega_0 t} |2\rangle\langle 0| \\ &\quad - \hbar\Omega_2 e^{-i\omega_2 t} |3\rangle\langle 2| - \hbar\Omega_3 e^{-i\omega_3 t} |4\rangle\langle 2| + \text{H.c.}, \end{aligned} \tag{3}$$

where $\hbar\nu_i$ denotes the energies of the levels $|i\rangle$ $(i = 0, 1, 2, 3, 4)$.

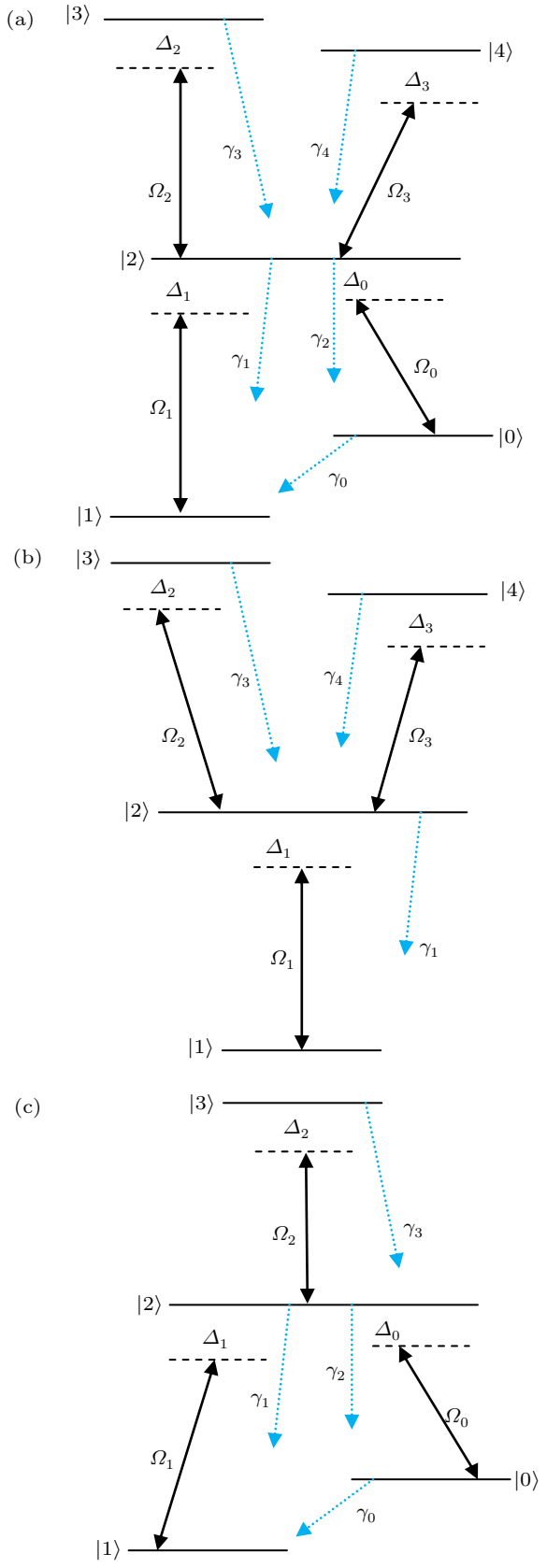


Fig. 2. (color online) Schematics of (a) five-level system in K-type configuration, (b) four-level system in Y-type configuration, (c) four-level system in inverted-Y-type configuration SDQWs.

The master equation of motion for the density operator in an arbitrary multi-level SDQW system can be written as

$$\frac{\partial \rho}{\partial t} = -\frac{\mathrm{i}}{\hbar}[H,\rho]. \tag{4}$$

Substituting Eqs. (2) and (3) into Eq. (4), the density matrix equations of motion for K-type SDQW medium can be obtained as

$$\begin{aligned}
\dot{\rho}_{12} &= -F_{12}\rho_{12} + \mathrm{i}\Omega_0\rho_{10} + \mathrm{i}\Omega_1(\rho_{11}-\rho_{22}) + \mathrm{i}\Omega_2\rho_{13} + \mathrm{i}\Omega_3\rho_{14},\\
\dot{\rho}_{02} &= -F_{02}\rho_{02} + \mathrm{i}\Omega_0(\rho_{00}-\rho_{22}) + \mathrm{i}\Omega_1\rho_{01} + \mathrm{i}\Omega_2\rho_{03} + \mathrm{i}\Omega_3\rho_{04},\\
\dot{\rho}_{23} &= -F_{23}\rho_{23} - \mathrm{i}\Omega_0\rho_{03} - \mathrm{i}\Omega_1\rho_{13} + \mathrm{i}\Omega_2(\rho_{22}-\rho_{33}) - \mathrm{i}\Omega_3\rho_{43},\\
\dot{\rho}_{24} &= -F_{24}\rho_{24} - \mathrm{i}\Omega_0\rho_{04} - \mathrm{i}\Omega_1\rho_{14} - \mathrm{i}\Omega_2\rho_{34} + \mathrm{i}\Omega_3(\rho_{22}-\rho_{44}),\\
\dot{\rho}_{10} &= -F_{10}\rho_{10} + \mathrm{i}\Omega_0\rho_{12} - \mathrm{i}\Omega_1\rho_{20},\\
\dot{\rho}_{13} &= -F_{13}\rho_{13} - \mathrm{i}\Omega_1\rho_{23} + \mathrm{i}\Omega_2\rho_{12},\\
\dot{\rho}_{14} &= -F_{14}\rho_{14} - \mathrm{i}\Omega_1\rho_{24} + \mathrm{i}\Omega_3\rho_{12},\\
\dot{\rho}_{03} &= -F_{03}\rho_{03} - \mathrm{i}\Omega_0\rho_{23} + \mathrm{i}\Omega_2\rho_{02},\\
\dot{\rho}_{04} &= -F_{04}\rho_{04} - \mathrm{i}\Omega_0\rho_{24} + \mathrm{i}\Omega_3\rho_{02},\\
\dot{\rho}_{34} &= -F_{34}\rho_{34} - \mathrm{i}\Omega_2\rho_{24} + \mathrm{i}\Omega_3\rho_{32},\\
\dot{\rho}_{00} &= -2\gamma_0\rho_{00} + 2\gamma_2\rho_{22} + \mathrm{i}\Omega_0(\rho_{02}-\rho_{20}),\\
\dot{\rho}_{11} &= 2\gamma_0\rho_{00} + 2\gamma_1\rho_{22} + \mathrm{i}\Omega_1(\rho_{12}-\rho_{21}),\\
\dot{\rho}_{33} &= -2\gamma_3\rho_{33} - \mathrm{i}\Omega_2(\rho_{23}-\rho_{32}),\\
\dot{\rho}_{44} &= -2\gamma_4\rho_{44} - \mathrm{i}\Omega_3(\rho_{24}-\rho_{42}),\\
\rho_{00} &+ \rho_{11} + \rho_{22} + \rho_{33} + \rho_{44} = 1,
\end{aligned} \tag{5}$$

where

$$\begin{aligned}
F_{10} &= \gamma_0 - \mathrm{i}(\Delta_1-\Delta_0), & F_{03} &= \gamma_0+\gamma_3 - \mathrm{i}(\Delta_0+\Delta_2),\\
F_{12} &= \gamma_1+\gamma_2 - \mathrm{i}\Delta_1, & F_{04} &= \gamma_0+\gamma_4 - \mathrm{i}(\Delta_0+\Delta_3),\\
F_{13} &= \gamma_3 - \mathrm{i}(\Delta_1+\Delta_2), & F_{23} &= \gamma_1+\gamma_2+\gamma_3 - \mathrm{i}\Delta_2,\\
F_{14} &= \gamma_4 - \mathrm{i}(\Delta_1+\Delta_3), & F_{24} &= \gamma_1+\gamma_2+\gamma_4 - \mathrm{i}\Delta_3,\\
F_{02} &= \gamma_0+\gamma_1+\gamma_2 - \mathrm{i}\Delta_0, & F_{34} &= \gamma_3+\gamma_4 - \mathrm{i}(\Delta_3-\Delta_2).
\end{aligned} \tag{6}$$

2.2. Y-type system

This system consists of four subbands that constitute a Y-type system as shown in Fig. 2(b).

Levels $|1\rangle$, $|2\rangle$, and $|3\rangle$ are in a usual three-level ladder-type configuration, while level $|2\rangle$ together with levels $|3\rangle$, $|4\rangle$ forms a three-level V-type configuration. So, this composite system consists of two sub-systems, i.e., ladder-type configuration and V-type configuration. All the parameters are defined as being similar to the K-type system, and the description of the optically allowed transitions in this system is similar to that in the K-type system without the zeroth level and the pumping field with amplitude ε_0. In a similar manner the equations of motion for the density matrix elements for the Y-type system read

$$\begin{aligned}
\dot{\rho}_{12} &= -F_{12}\rho_{12} + \mathrm{i}\Omega_1(\rho_{11}-\rho_{22}) + \mathrm{i}\Omega_2\rho_{13} + \mathrm{i}\Omega_3\rho_{14},\\
\dot{\rho}_{23} &= -F_{23}\rho_{23} - \mathrm{i}\Omega_1\rho_{13} + \mathrm{i}\Omega_2(\rho_{22}-\rho_{33}) - \mathrm{i}\Omega_3\rho_{43},\\
\dot{\rho}_{24} &= -F_{24}\rho_{24} - \mathrm{i}\Omega_1\rho_{14} - \mathrm{i}\Omega_2\rho_{34} + \mathrm{i}\Omega_3(\rho_{22}-\rho_{44}),
\end{aligned}$$

$$
\begin{aligned}
\dot{\rho}_{13} &= -F_{13}\rho_{13} - \mathrm{i}\Omega_1\rho_{23} + \mathrm{i}\Omega_2\rho_{12},\\
\dot{\rho}_{14} &= -F_{14}\rho_{14} - \mathrm{i}\Omega_1\rho_{24} + \mathrm{i}\Omega_3\rho_{12},\\
\dot{\rho}_{34} &= -F_{34}\rho_{34} - \mathrm{i}\Omega_2\rho_{24} + \mathrm{i}\Omega_3\rho_{32},\\
\dot{\rho}_{11} &= 2\gamma_1\rho_{22} + \mathrm{i}\Omega_1(\rho_{12} - \rho_{21}),\\
\dot{\rho}_{33} &= -2\gamma_3\rho_{33} - \mathrm{i}\Omega_2(\rho_{23} - \rho_{32}),\\
\dot{\rho}_{44} &= -2\gamma_4\rho_{44} - \mathrm{i}\Omega_3(\rho_{24} - \rho_{42}),\\
\rho_{11} &+ \rho_{22} + \rho_{33} + \rho_{44} = 1.
\end{aligned} \tag{7}
$$

2.3. Inverted-Y-type system

This system consists of four levels that constitute an inverted-Y-type system as shown in Fig. 2(c). Levels $|1\rangle$, $|2\rangle$, and $|3\rangle$ are again in a usual three-level ladder-type configuration, whereas level $|2\rangle$ together with levels $|0\rangle$, $|1\rangle$ forms a three-level Λ-type configuration Thus, in contrast to Subsection 2.2, this composite system consists of two subsystems, i.e., ladder-type configuration and Λ-type configuration. Again, the description of the optically allowed transitions in this system and the defined parameters are similar to those in the K-type system, but without the fourth level and the pumping field with amplitude ε_3. The equations of motion for the density matrix elements for the inverted Y-type system in a similar manner read

$$
\begin{aligned}
\dot{\rho}_{12} &= -F_{12}\rho_{12} + \mathrm{i}\Omega_0\rho_{10} + \mathrm{i}\Omega_1(\rho_{11} - \rho_{22}) + \mathrm{i}\Omega_2\rho_{13},\\
\dot{\rho}_{02} &= -F_{02}\rho_{02} + \mathrm{i}\Omega_0(\rho_{00} - \rho_{22}) + \mathrm{i}\Omega_1\rho_{01} + \mathrm{i}\Omega_2\rho_{03},\\
\dot{\rho}_{23} &= -F_{23}\rho_{23} - \mathrm{i}\Omega_0\rho_{03} - \mathrm{i}\Omega_1\rho_{13} + \mathrm{i}\Omega_2(\rho_{22} - \rho_{33}),\\
\dot{\rho}_{10} &= -F_{10}\rho_{10} + \mathrm{i}\Omega_0\rho_{12} - \mathrm{i}\Omega_1\rho_{20},\\
\dot{\rho}_{13} &= -F_{13}\rho_{13} - \mathrm{i}\Omega_1\rho_{23} + \mathrm{i}\Omega_2\rho_{12},\\
\dot{\rho}_{03} &= -F_{03}\rho_{03} - \mathrm{i}\Omega_0\rho_{23} + \mathrm{i}\Omega_2\rho_{02},\\
\dot{\rho}_{00} &= -2\gamma_0\rho_{00} + 2\gamma_2\rho_{22} + \mathrm{i}\Omega_0(\rho_{02} - \rho_{20}),\\
\dot{\rho}_{11} &= 2\gamma_0\rho_{00} + 2\gamma_1\rho_{22} + \mathrm{i}\Omega_1(\rho_{12} - \rho_{21}),\\
\dot{\rho}_{33} &= -2\gamma_3\rho_{33} - \mathrm{i}\Omega_2(\rho_{23} - \rho_{32}),\\
\rho_{00} &+ \rho_{11} + \rho_{22} + \rho_{33} = 1.
\end{aligned} \tag{8}
$$

3. Optical bistability, theory and equations

The density matrix equations (5), (7), (8) can be solved to obtain the steady state response of the medium. The susceptibility of the system for a weak probe field is determined by coherence term ρ_{21}

$$\chi = \frac{2N\wp}{E\varepsilon_0}\rho_{21}, \tag{9}$$

where N is the QW number density in the medium. Here, the imaginary part of susceptibility χ ($\chi = \chi' + \mathrm{i}\chi''$) corresponds to the absorption for the probe field.

Now, we put the ensemble of M homogeneously K-type (Y-type, or inverted-Y-type) QW molecules in a unidirectional ring cavity as shown in Fig. 1(c). The intensity reflection and transmission coefficients of mirrors 1 and 2 are R and T (with $R + T = 1$), respectively. We assume that both the mirrors 3 and 4 are perfect reflectors. The total electromagnetic field seen by N homogeneous QW molecules contained in cell of length L can be written as

$$
\begin{aligned}
\varepsilon &= \varepsilon_1 \mathrm{e}^{-\mathrm{i}\omega_1 t} + \varepsilon_0 \mathrm{e}^{-\mathrm{i}\omega_0 t} + \varepsilon_2 \mathrm{e}^{-\mathrm{i}\omega_2 t}\\
&\quad + \varepsilon_3 \mathrm{e}^{-\mathrm{i}\omega_3 t} + \text{c.c.}, \ \text{(K-type)},\\
\varepsilon &= \varepsilon_1 \mathrm{e}^{-\mathrm{i}\omega_1 t} + \varepsilon_2 \mathrm{e}^{-\mathrm{i}\omega_2 t}\\
&\quad + \varepsilon_3 \mathrm{e}^{-\mathrm{i}\omega_3 t} + \text{c.c.}, \ \text{(Y-type)},\\
\varepsilon &= \varepsilon_1 \mathrm{e}^{-\mathrm{i}\omega_1 t} + \varepsilon_0 \mathrm{e}^{-\mathrm{i}\omega_0 t}\\
&\quad + \varepsilon_2 \mathrm{e}^{-\mathrm{i}\omega_2 t} + \text{c.c.}, \ \text{(inverted-Y-type)}.
\end{aligned} \tag{10}
$$

Under slowly varying envelope approximation, the dynamic response of the probe field is governed by Maxwell's equations,

$$\frac{\partial\varepsilon_1}{\partial t} + c\frac{\partial\varepsilon_1}{\partial z} = \frac{\mathrm{i}\omega_1}{2\varepsilon_0}P(\omega_1), \tag{11}$$

where $P(\omega_1)$ is the induced polarization in the transition $|1\rangle \leftrightarrow |2\rangle$ and is given by

$$P(\omega_1) = N\mu_{12}(\rho_{21}). \tag{12}$$

In the steady state regime, the term containing $\partial/(\partial t)$ in Eq. (11) is equal to zero. Substituting Eq. (12) into Eq. (11), we obtain the field amplitude relation as

$$\frac{\partial\varepsilon_1}{\partial z} = \mathrm{i}\frac{N\omega_1\mu_{12}}{2c\varepsilon_0}(\rho_{21}). \tag{13}$$

The coherent field $\varepsilon_1^{\mathrm{I}}$ enters into the cavity through the mirror M_1, interacts with the QW sample of length L, circulates in the cavity, and partially comes out of the mirror M_2 as $\varepsilon_1^{\mathrm{T}}$. The probe field at the start of SDQW sample is $\varepsilon_1(0)$ and propagates to the end of the SDQW sample and becomes $\varepsilon_1^{\mathrm{L}}$ in the single pass transition. The coupling fields can also enter into the cavity through the polarizing beam splitter and co-propagates with the cavity field in the QW nanostructure cell. For a perfectly tuned cavity, the boundary conditions in the steady-state limit between the incident field $\varepsilon_1^{\mathrm{I}}$ and transmitted field $\varepsilon_1^{\mathrm{T}}$ are[57]

$$\varepsilon_1(L) = \frac{\varepsilon_1^{\mathrm{T}}}{\sqrt{T}}, \tag{14a}$$

$$\varepsilon_1(0) = \sqrt{T}\varepsilon_1^{\mathrm{I}} + R\varepsilon_1(L), \tag{14b}$$

where L is the length of the QW sample. Note that R is the feedback mechanism due to the reflection from the mirror M_2. It is responsible for the bistable behavior, so we do not expect any bistability when $R = 0$ in Eq. (14b). According to the mean-field limit[58] and by using the boundary condition, the steady state behavior of transmitting field is given by

$$y = 2x - \mathrm{i}C(\rho_{21}), \tag{15}$$

where $y = \mu_{12}\varepsilon_1^{\mathrm{I}}/(\hbar\sqrt{T})$ and $x = \mu_{12}\varepsilon_1^{\mathrm{T}}/(2\hbar\sqrt{T})$ are the normalized input and output field, respectively. The parameter

$C = NL\omega_1\mu_{12}^2/(2\hbar c\varepsilon_0 T)$ is the cooperatively parameter for QWs in a ring cavity. Transmitted field depends on the incident probe field and the coherence term ρ_{21} via Eq. (15). So, the bistable behavior of the medium can be determined by the QW sample variables through ρ_{21}. We set the time derivatives of ρ_{ij} to be equal to zero, i.e.,

$$\partial\rho_{ij}/(\partial t) = 0 \quad (i, j = 1, 2, 3, 4)$$

in Eq. (5) for K-type configuration (Eq. (7) for Y-type configuration or Eq. (8) for inverted Y-type configuration) and solve the corresponding density matrix equations together with the coupled field Eq. (15).

4. Numerical simulations and discussion

4.1. Controllable OB in K-type SDQW medium

Now, we start with the analysis of the K-type SDQW system for studying the steady state behaviors of the output field intensity versus the input field intensity for various parameters illustrated in Figs. 3–7. At first, we analyze the dependence of the shift of OB hysteresis curve on the wavelength detuning λ_0 caused by the probe field for the parametric condition: $\gamma_2/\gamma_1 = \gamma_3/\gamma_1 = \gamma_4/\gamma_1 = 1$, $\gamma_0/\gamma_1 = 0.2, \Omega_0/\gamma_1 = \Omega_2/\gamma_1 = \Omega_3/\gamma_1 = 1$, and in the resonance condition $\Delta_0/\gamma_1 = \Delta_2/\gamma_1 = \Delta_3/\gamma_1 = 0$. We find that the hysteresis curve shifts toward the right or left correspond to the increase or decrease in the OB threshold intensity which is illustrated in Fig. 3. Three different behaviors of OB profile are observed when we investigate the effect of probe wavelength λ_0. Figure 3(a) shows that increasing the probe wavelength from $\lambda_0 = 1542$ nm to $\lambda_0 = 1546$ nm leads to the increase in the threshold intensity. For the next range of wavelengths, we observe different behaviors. It is shown that for $\lambda_0 = 1548$ nm the OB threshold intensity finds its maximal value, then it reduces for $\lambda_0 = 1550$ nm and again the OB threshold increases for larger wavelengths, like $\lambda_0 = 1551$ nm. This condition is displayed in Fig. 3(b). The effect of the third range of wavelengths is illustrated in Fig. 3(c). Obviously, by more increasing the λ_0, the threshold of optical bistability can be efficiently reduced again. We can explain the reason for this phenomenon as follows. Increasing λ_0 can modify the absorption and the nonlinearity of medium and thus makes the cavity field easier or harder to reach saturation. The plot of the absorption profile in Fig. 4 may be beneficial to understanding the physical origin of such an effect. We calculated the values of the probe absorption for each particular wavelength and the results are given in Table 1. These values manifest the origin for the increase or decrease in the OB threshold. In fact, the main reason for the large bistable threshold may be attributed to the presence of a strong absorption in the medium which makes the field hard to reach saturation, while a reduced probe absorption in the SDQW sample makes the field easier to be saturated and so, the OB threshold will be remarkably reduced.

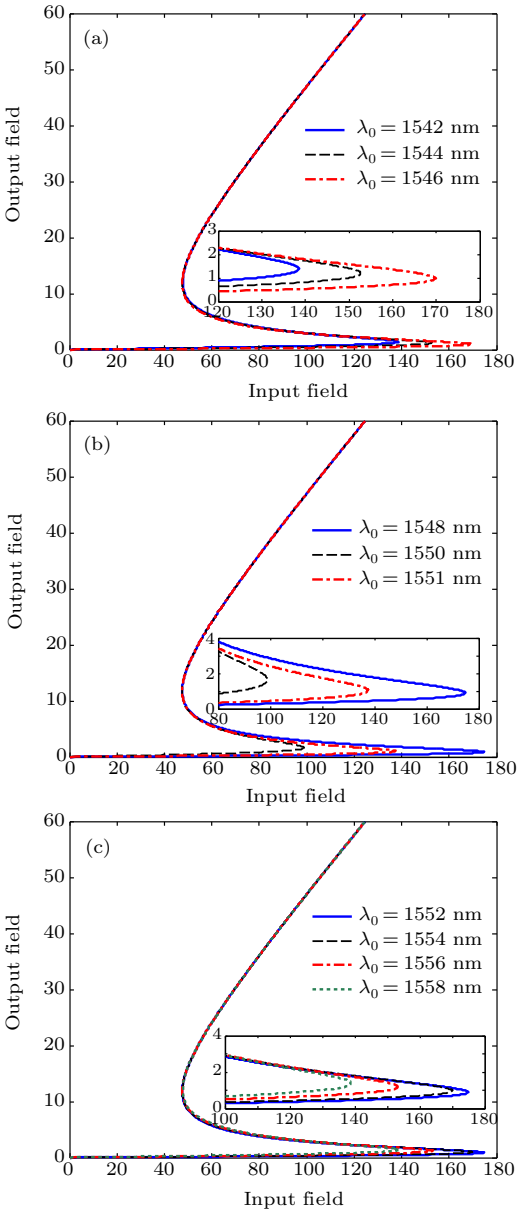


Fig. 3. (color online) Plots of the output field intensity against the input field intensity for different values of the probe wavelength detuning λ_0. The selected parameters are $\gamma_2/\gamma_1 = \gamma_3/\gamma_1 = \gamma_4/\gamma_1 = 1\gamma_0/\gamma_1 = 0.2, \Omega_0/\gamma_1 = \Omega_2/\gamma_1 = \Omega_3/\gamma_1 = 1, \Delta_0/\gamma_1 = \Delta_2/\gamma_1 = \Delta_3/\gamma_1 = 0, \lambda_0 =$ 1550 nm.

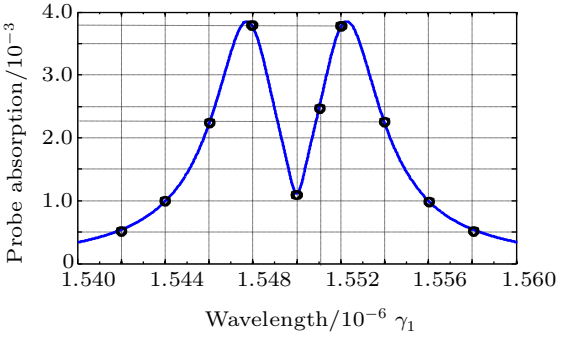


Fig. 4. (color online) Probe absorption versus probe wavelength detuning λ_0. Here, $\Omega_1/\gamma_1 = 0.01$, and the selected parameters are the same as those in Fig. 3.

It is desirable to reduce the threshold of optical bistability through proper tuning of coupling fields intensities. For this

purpose, we show the plots of the output field intensity against the input field intensity for different values of the coupling field intensities Ω_0, Ω_2, Ω_3 in Figs. 5(a), 5(c), and 5(e). It is clearly shown that when keeping all other parameters fixed, and increasing each of the Rabi frequencies Ω_0, Ω_2 or Ω_3, the threshold of the optical bistability decreases progressively and the area of the hysteresis loop becomes narrower. The gradual increasing of the Rabi frequencies gives rise to the reduction of the absorption for the probe laser field on the transition $|1\rangle \leftrightarrow |2\rangle$, and finally EIT appears as shown in Figs. 5(b), 5(d), and 5(f), which makes the cavity field easier to reach saturation.

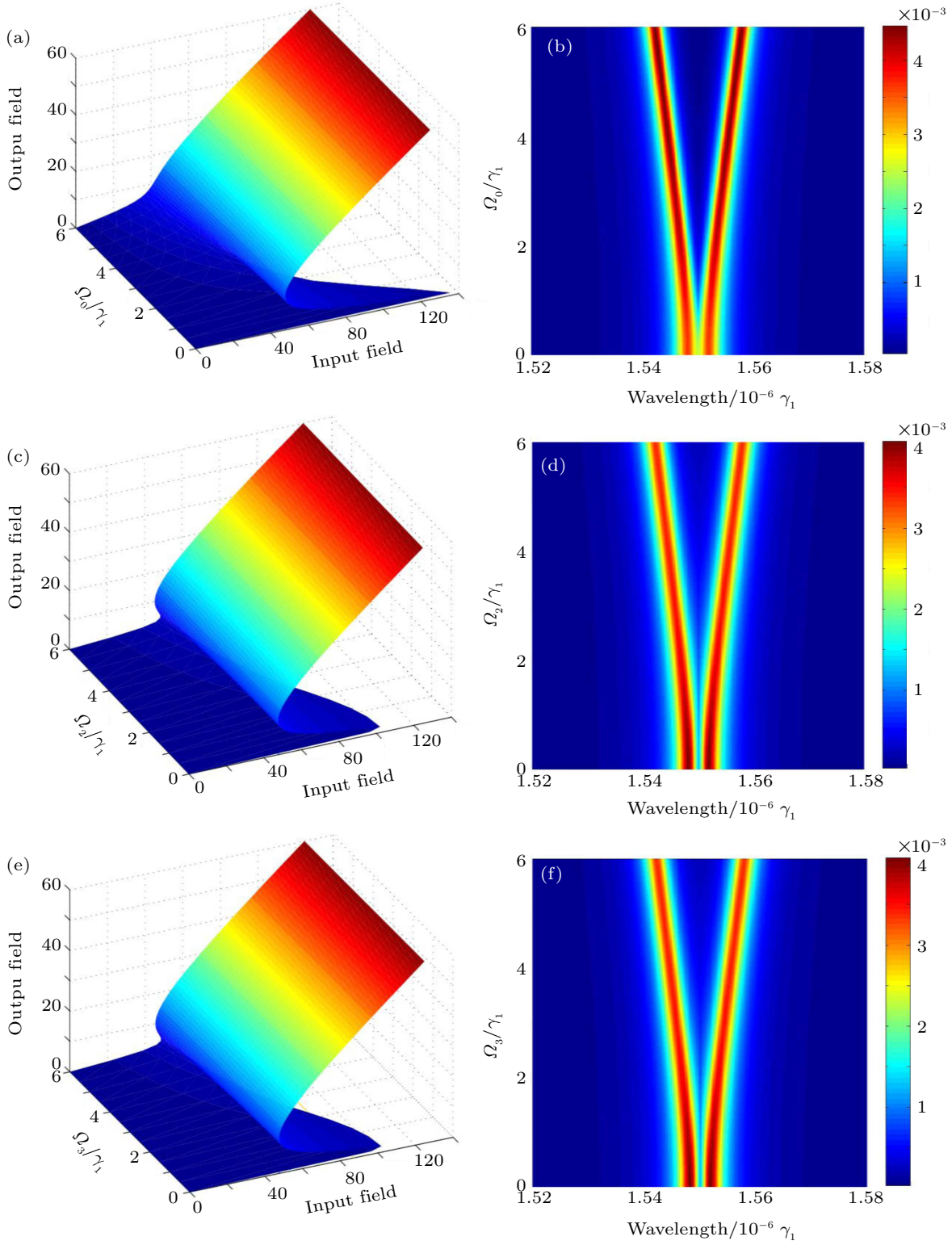


Fig. 5. (color online) Three-dimensional (3D) plots of the output field intensity against the input field intensity and the coupling field intensities $\Omega_0, \Omega_2, \Omega_3$ ((a), (c), and (e)). Contour plots of the steady-state probe absorption spectra versus coupling field intensities $\Omega_0, \Omega_2, \Omega_3$ and probe wavelength detuning λ_0 ((b), (d), and (f)). The selected parameters are the same as those in Fig. 3.

Table 1. Calculated values of probe absorption for different values of probe wavelength detuning λ_0.

λ_0/nm	1542	1544	1546	1548	1550	1551	1552	1554	1556	1558
$\mathrm{Im}\rho_{21}/10^{-3}$	0.5	1	2.3	3.8	1.11	2.5	3.8	2.3	1	0.5

The behaviors of OB with different values of the cooperation parameter C is displayed in Fig. 6. It is self-explaining that OB is seen when the cooperation parameter C is large. We can observe that the threshold increases as value of parameter C increases from small value to the larger value. It is known that the cooperation parameter C is directly proportional to the electron number density N. Thus, the enhancement in the probe absorption of the QW sample as the number density of electrons increases could be explained as the raise of the threshold intensity with the cooperation parameter C.

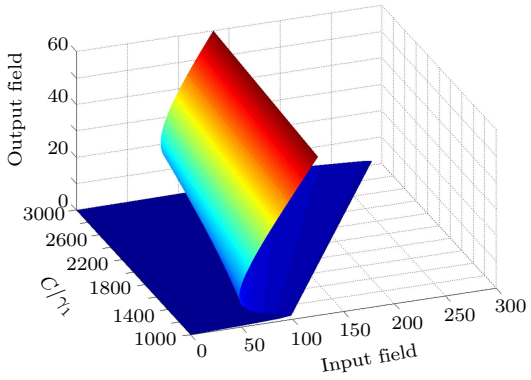


Fig. 6. (color online) 3D plot of the output field intensity against the input field intensity and the electronic cooperation parameter C. The selected parameters are the same as those in Fig. 3.

4.2. Comparison of OB features in K-type, Y-type, and inverted Y-type SDQW media

Now, we turn to compare the OB features of K-type, Y-type, and inverted Y-type SDQW schemes. In order to demonstrate the OB controllability in this solid configuration, the behaviors of the output field intensity in the steady state with respect to the change of input field intensity are illustrated in Fig. 7(a) for K-type, Y-type, and inverted Y-type QW schemes. Here we take $\Omega_0/\gamma = \Omega_2/\gamma = \Omega_3/\gamma = 1$ for the K-type system, $\Omega_0/\gamma = \Omega_2/\gamma = 1$ ($\Omega_3/\gamma = 0$) for the inverted Y-type, and $\Omega_2/\gamma = \Omega_3/\gamma = 1$ ($\Omega_0/\gamma = 0$) for the Y-type QW configuration respectively. It is readily found that

$$\begin{aligned}\text{OB threshold}^{\lambda_0=1550\text{ nm}}_{\text{Y-type}} &< \text{OB threshold}^{\lambda_0=1550\text{ nm}}_{\text{inverted Y-type}},\\ &< \text{OB threshold}^{\lambda_0=1550\text{ nm}}_{\text{K-type}}.\end{aligned}$$

In Fig. 7(b), we compare the values of the probe absorption at the line center ($\lambda_0 = 1550$ nm) for each scheme. It is obvious that

$$\begin{aligned}\text{Probe absorption}^{\lambda_0=1550\text{ nm}}_{\text{Y-type}} &< \text{Probe absorption}^{\lambda_0=1550\text{ nm}}_{\text{inverted Y-type}},\\ &< \text{Probe absorption}^{\lambda_0=1550\text{ nm}}_{\text{K-type}},\end{aligned}$$

which indicates that the cavity field more easily reaches saturation for the Y-type SDQW medium, while it will be harder to saturate in K-type QW medium.

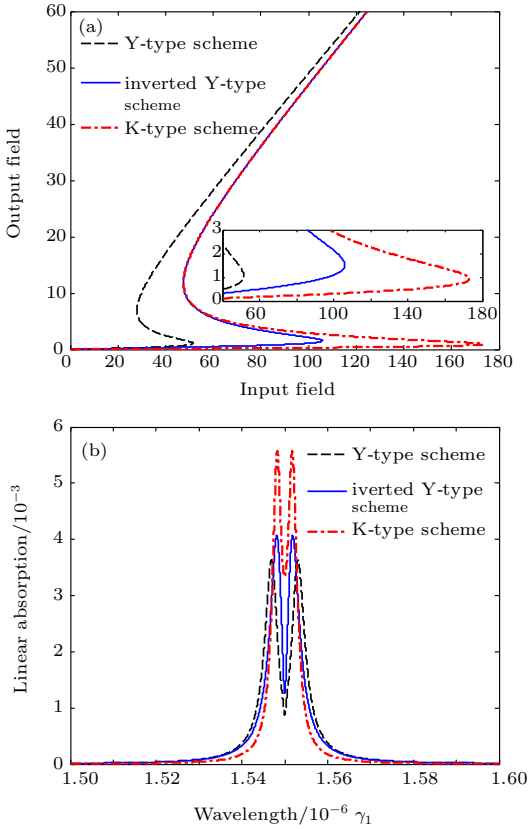


Fig. 7. (color online) (a) Plots of the output field intensity against the input field intensity, and (b) plots of probe absorption versus probe wavelength detuning λ_0 for different SDQW schemes (K-, Y-, and inverted Y-type SDQWs).

5. Conclusions

In this work, the OB behaviour of a K-type SDQW system contained in a unidirectional ring cavity is theoretically explored. The influences of the optical control fields and probe wavelength on optical bistability of the medium are studied. The comparisons among OB features of K-type, Y-type, and inverted Y-type configurations which can occur in this SDQW system are then discussed. The SDQW medium investigated in the presented work is a solid with flexible design, so, it may open up an avenue to exploring the possibilities for nonlinear optics and quantum information processing in condensed-state matters, and give rise to substantial influence on technology.

References

[1] Chen Z, Du C, Gong S and Xu Z 1999 *Phys. Lett. A* **259** 15
[2] Rosenberger A T, Orozco L A, Kimble H J and Drummond P D 1991 *Phys. Rev. A* **43** 6284
[3] Harris S E 1997 *Phys. Today* **50** 36
[4] Wu Y and Yang X X 2005 *Phys. Rev. A* **71** 053806
[5] Wu Y and Yang X X 2007 *Phys Rev. Lett.* **98** 013601
[6] Wan R G, Kou J, Jiang L, Jiang Y and Gao J Y 2011 *Phys. Rev. A* **83** 033824

[7] Hamedi H R, Radmehr Arash and Sahrai M 2014 *Phys. Rev. A* **90** 053836
[8] Deng L and Payne M G 2007 *Phys. Rev. Lett.* **98** 253902
[9] Ding C L, Li J H, Yang X X, Zhang D and Xiong H 2011 *Phys. Rev. A* **84** 043840
[10] Wang Z P and Yu B L 2014 *Laser Phys. Lett.* **11** 035201
[11] Wu Y and Yang X X 2004 *Phys. Rev. A* **70** 053818
[12] Niu Y P, Gong S Q, Li R X, Xu Z Z and Liang X Y 2005 *Opt. Lett.* **30** 3371
[13] Cheng D C, Liu C P and Gong S Q 2004 *Phys. Lett. A* **332** 244
[14] Sun H, Niu Y P, Jin S Q and Gong S Q 2008 *J. Phys. B: At. Mol. Opt. Phys.* **41** 065504
[15] Wang Z P and Yu B L 2013 *J. Appl. Phys.* **113** 113101
[16] Harris S E and Hau Lene Vestergaard 1999 *Phys. Rev. Lett.* **82** 4611
[17] Imamoḡlu A, Schmidt H, Woods G and Deutsch M 1997 *Phys. Rev. Lett.* **79** 1467
[18] Niu Y P and Gong S Q 2006 *Phys. Rev. A* **73** 053811
[19] Jiang W J, Yan X A, Song J P, Zheng H B, Wu C X, Yin B Y and Zhang Y P 2009 *Opt. Commun.* **282** 101
[20] Zhu Z W, Xue S Z, Wu Y M, *et al.* 2012 *Chin. Phys. Lett.* **29** 037802
[21] Yang J J, Li H J, Wen W and Huang G X 2012 *Acta Phys. Sin.* **61** 224204 (in Chinese)
[22] Wang Z, Chen A X, Bai Y F, Yang W X and Lee R K 2012 *J. Opt. Soc. Am. B* **29** 2891
[23] Wu J W and Bikash N 2013 *Chin. Phys. B* **22** 084204
[24] Zhang H J, Guo H J, Sun H, *et al.* 2013 *Chin. Phys. B* **22** 104208
[25] Hamedi H R 2014 *Appl. Opt.* **53** 5391
[26] Cheng D C, Liu C P and Gong S Q 2006 *Opt. Commun.* **263** 111
[27] Mehmannavaz M R, Nasehi R, Sattari H and Mahmoudi M 2014 *Superlattices and Microstructures* **75** 27
[28] Li X L, Zhang L S, Sun J and Feng X M 2012 *Acta Phys. Sin.* **61** 044202 (in Chinese)
[29] Phillips M C and Wang H L 2003 *Phys. Rev. Lett.* **91** 183602
[30] Wagner M, Schneider H, Stehr D, Winnerl S, Andrews A M, Schartner S, Strasser G and Helm M 2010 *Phys. Rev. Lett.* **105** 167401
[31] Wu Y, Saldana J and Zhu Y 2003 *Phys. Rev. A* **67** 013811
[32] Kang H, Park Y H, Sohu I B and Jeong M S 2011 *Opt. Commun.* **284** 1045
[33] Asadpour S H, Hamedi H R, Eslami-Majd A and Sahrai M 2011 *Physica E* **44** 464
[34] Yang W X, Zha T T and Lee R K 2009 *Phys. Lett. A* **374** 355
[35] Sun H, Gong S Q, Niu Y P, Jin S Q, Li R X and Xu Z Z 2006 *Phys. Rev. B* **74** 155314
[36] Li J H 2007 *Phys. Rev. B* **75** 155329
[37] Ai J F, Chen A X and Deng L 2013 *Chin. Phys. B* **22** 024209
[38] Wang Z P 2009 *Opt. Commun.* **282** 4745
[39] Wijewardane H O and Ullrich C A 2004 *Appl. Phys. Lett.* **84** 3984
[40] Joshi A and Xiao M 2004 *Appl. Phys. B* **79** 65
[41] Shui T, Wang Z P and Yu B L 2014 *Phys. Lett. A* **378** 235
[42] Wang Z P, Yu B L, Xu F and Zhen S L 2013 *Appl. Phys. A* **112** 443
[43] Hamedi H R 2014 *Physica B* **450** 128
[44] Hao X Y, Ding C L, Lu X Y, Li J H and Yang X X 2010 *Physica E* **42** 1984
[45] Wu J, Yu R and Li J H 2010 *Opt. Commun.* **283** 5067
[46] Shen H Z, Qin M and Yi X X 2013 *Phys. Rev. A* **88** 033835
[47] Faist J, Capasso F, Sirtori C, Hutchinson A L, West K W and Pfeiffer L N 1997 *Appl. Phys. Lett.* **71** 3477
[48] Faist J, Sirtori C, Capasso F, Pfeiffer L and West K W 1994 *Appl. Phys. Lett.* **64** 872
[49] Hao X, Yang W X, Lu X, Liu J, Huang P, Ding C and Yang X 2008 *Phys. Lett. A* **372** 7081
[50] Osman K I, Hassan S S and Joshi A 2009 *Eur. Phys. J. D* **54** 119
[51] Faist J, Sirtori C, Capasso F, Hutchinson A L, Pfeiffer L and West K W 1996 *Opt. Lett.* **21** 985
[52] Serapiglia G B, Paspalakis E, Sirtori C, Vodopyanov K L and Phillips C C 2000 *Phys. Rev. Lett.* **84** 1019
[53] Dynes J F, Frogley M D, Beck M, Faist J and Phillips C C 2005 *Phys. Rev. Lett.* **94** 157403
[54] Wu J H, Gao J Y, Xu J H, Silvestri L, Artoni M, La Rocca G C and Bassani F 2005 *Phys. Rev. Lett.* **95** 057401
[55] Kapale K T, Marlan O S, Zhu S Y and Zubairy M S 2003 *Phys. Rev. A* **67** 023804
[56] Gardiner C W and Collett M J 1985 *Phys. Rev. A* **31** 3761
[57] Lugiato L A 1984 in: Wolf E (ed.) *Progress in Optics* (Amsterdam: North-Holland) p. 71
[58] Rosenberger A T, Orozco L A and Kimble H J 1983 *Phys. Rev. A* **28** 2529